THE JOURNAL OF PHYSICAL CHEMISTRY A
A JOURNAL OF THE AMERICAN CHEMICAL SOCIETY

pubs.acs.org/JPCA Article

Nitrogen-15 and Fluorine-19 Relaxation Dynamics and Spin-Relayed SABRE-SHEATH Hyperpolarization of Fluoro-[$^{15}N_3$]metronidazole

Mohammad S. H. Kabir,* Sameer M. Joshi, Anna Samoilenko, Isaiah Adelabu, Shiraz Nantogma, Juri G. Gelovani, Boyd M. Goodson, and Eduard Y. Chekmenev*

Cite This: https://doi.org/10.1021/acs.jpca.3c02317 Read Online

ABSTRACT: Efficient ^{15}N-hyperpolarization of [$^{15}N_3$]-metronidazole was reported previously using the Signal Amplification By Reversible Exchange in SHield Enabled Alignment Transfer (SABRE-SHEATH) technique. This hyperpolarized FDA-approved antibiotic is a potential contrast agent because it can be administered in a large dose and because previous studies revealed long-lasting HP states with exponential decay constant T_1 values of up to 10 min. Possible hypoxia-sensing applications have been proposed using hyperpolarized [$^{15}N_3$]metronidazole. In this work, we report on the functionalization of [$^{15}N_3$]metronidazole with a fluorine-19 moiety via a one-step reaction to substitute the −OH group. SABRE-SHEATH hyperpolarization studies of fluoro-[$^{15}N_3$]metronidazole revealed efficient hyperpolarization of all three ^{15}N sites with maximum $\%P_{15N}$ values ranging from 4.2 to 6.2%, indicating efficient spin-relayed polarization transfer in microtesla fields via the network formed by $^2J_{15N\text{-}15N}$. The corresponding ^{15}N to ^{19}F spin-relayed polarization transfer was found to be far less efficient with $\%P_{19F}$ of 0.16%, i.e., more than an order of magnitude lower than that of ^{15}N. Relaxation dynamics studies in microtesla fields support a spin-relayed polarization transfer mechanism because all ^{15}N and ^{19}F spins share the same T_1 value of ca. 16−20 s and the same magnetic field profile for the SABRE-SHEATH polarization process. We envision the use of fluoro-[$^{15}N_3$]metronidazole as a potential hypoxia sensor. It is anticipated that under hypoxic conditions, the nitro group of fluoro-[$^{15}N_3$]metronidazole undergoes electronic stepwise reduction to an amino derivative. Ab initio calculations of ^{15}N and ^{19}F chemical shifts of fluoro-[$^{15}N_3$]metronidazole and its putative hypoxia-induced metabolites clearly indicate that the chemical shift dispersions of all three ^{15}N sites and the ^{19}F site are large enough to enable the envisioned hypoxia-sensing approaches.

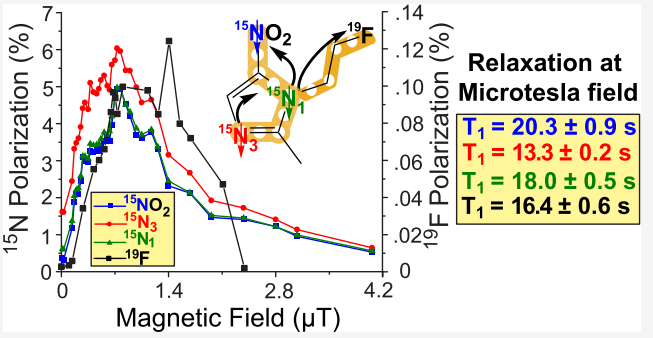

INTRODUCTION

NMR hyperpolarization techniques increase nuclear spin polarization (P) to the order of unity, compared to equilibrium P, which is on the order of 10^{-5} (or 10^{-3}%) for proton nuclear spins at a clinically relevant magnetic field of 3 T.[1,2] Since NMR signal scales linearly with P, this dramatic gain in nuclear spin polarization is readily realized by 4−5 orders of magnitude increase of NMR and MRI signals.[1] Hyperpolarized (HP) elements and molecules can be employed for a wide range of applications including bioimaging applications, which remain the key driver behind the development of hyperpolarization techniques.[3,4] Indeed, HP ^{129}Xe was recently cleared by FDA for use as an inhalable contrast agent for pulmonary ventilation imaging in December 2022. Typically, HP contrast agents can be administered via inhalation of HP gas (e.g., HP ^{129}Xe[3,5−8]) or injection of HP liquid (e.g., [1-^{13}C]pyruvate).[9,10]

The key motivation for the development of injectable HP contrast agents is their utility for tracking metabolic transformation through the changes of the chemical shift of the injected HP probe and its metabolite(s).[11−13] Combined with the fact that MRI employs no ionizing radiation, HP MRI is a next-generation molecular imaging technology that offers multiple advantages over positron emission tomography (PET) radioactive tracers employed in modern-day clinical molecular imaging.[14,15]

One group of PET tracers employs nitroimidazole moieties tagged with radioactive [^{18}F] nuclei.[16] ^{18}F-fluoromisonidazole (^{18}F-FMISO) is a representative member of this family of PET tracers.[16−19] This PET imaging approach is based on the hypoxia-induced upregulation of 1-electron-type nitro-reductases (i.e., Cytochrome P_{450} 1A1 (CYP1A1), Cytochrome P_{450} 1A2 (CYP1A2), and CYP1B1) that reduce the nitro group of ^{18}F-FMISO to an amino group. As a result,^{18}F-FMISO is

Received: April 6, 2023
Revised: May 19, 2023

selectively trapped by hypoxic cells after its reduction in a low-oxygen environment.[20] Once ^{18}F-FMISO is cleared from the surrounding nonhypoxic tissues, the uptake of ^{18}F-FMISO can be readily detected, thereby enabling molecular imaging of hypoxia.[17−19] Hypoxia has been linked with neurodegeneration.[21] Moreover, hypoxia is a common feature in many cancers, and tumor hypoxia has also been associated with aggressive forms of cancer.[22] Hypoxic cancers are often more difficult to treat.[23] Because early detection of hypoxia can potentially lead to better treatment outcomes, an efficient molecular imaging modality for clinical hypoxia imaging is greatly desired.

Nitroimidazole-based PET tracers have been successfully employed in clinical research for detecting tumor hypoxia in breast and brain cancers.[24] Even though ^{18}F-FMISO PET is a promising technique for hypoxia imaging, it has some limitations that may substantially impact its clinical utility. First, similarly to other PET tracers such as [^{18}F]-fluorodeoxyglucose (^{18}F-FDG), ^{18}F-FMISO also employs a radioactive isotope. Moreover, it takes 2−3 h to clear ^{18}F-FMISO from the surrounding tissues,[25] which is comparatively longer compared to FDG clearance time of less than 1 h. Since PET scan cannot differentiate between metabolized and unmetabolized [^{18}F]FMISO, the clearance time is fundamentally unavoidable. Furthermore, the use of PET tracers requires advanced and costly infrastructure for the production, distribution, and administration of radioactive [^{18}F]-labeled compounds, which is a clear limitation of modern-day molecular imaging technology. A more efficient, cost-effective, and nonionizing molecular imaging modality is needed to establish such a next-generation molecular imaging technique.

We previously proposed a new solution to this key limitation of [^{18}F]FMISO PET scanning through the use of ^{15}N-hyperpolarized nitroimidazole derivatives,[26] i.e., using the same biochemistry that [^{18}F]FMISO exploits, but with two key differences: (1) Instead of using radioactive nuclides, we proposed to employ HP ^{15}N nuclei in metabolic contrast agents. (2) Previous theoretical studies revealed that hypoxia-induced metabolism of ^{15}N-labeled nitroimidazole probe can be readily sensed through large (tens to hundreds of ppm) changes in ^{15}N chemical shifts.[27] Since a metabolized molecular probe based on similar chemistry can in principle be readily differentiated in HP MRI, the requirement for the agent's long clearance from the surrounding tissues can be obviated. Taken together, these features of the approach potentially pave the way to fast metabolic scans of hypoxia without the use of ionizing radiation.

The key limitation of ^{15}N magnetic resonance is the overall low detection sensitivity of the ^{15}N nucleus—even in the HP state. Although a number of ^{15}N HP contrast agents have been developed to date, only a handful of in vivo studies have been reported because of this limitation.[28,29] The low detection sensitivity of ^{15}N stems from a low gyromagnetic ratio, γ_{15N}, which is 10 times lower than that of protons, and 2.5 times lower than that of ^{13}C. The HP MRI signal scales quadratically with γ, making ^{15}N approximately 6 times less sensitive than ^{13}C, and 100 times less sensitive than ^{1}H. One potential solution to circumvent the ^{15}N sensitivity challenge is to use proton sensing of ^{15}N HP states.[30,31] However, pilot in vivo studies with indirect sensing revealed challenges associated with proton background signals.[32,33]

We propose the use of indirect sensing of ^{15}N HP state via ^{19}F signal readout. Unlike the large physiological background of water protons, the ^{19}F has virtually no background signal. Moreover, the value of γ_{19F} is ∼0.93·γ_H, and the ^{19}F has a nearly 100% natural abundance, making it a sensitive detection nucleus. In this work, we report on the first steps toward this long-term goal. We functionalized [$^{15}N_3$]metronidazole with an ^{19}F moiety via a one-step reaction to substitute the −OH group. We employed the synthesized fluoro-[$^{15}N_3$]-metronidazole to perform Signal Amplification By Reversible Exchange in SHield Enables Alignment Transfer to Heteronuclei (SABRE-SHEATH)[34] hyperpolarization and relaxation dynamics studies of ^{15}N and ^{19}F nuclei. We additionally performed ab initio computational studies of ^{15}N and ^{19}F chemical shifts of putative metabolites of fluoro-[$^{15}N_3$]-metronidazole reduction during metabolism by hypoxic tissues with the perspective of chemical shift hypoxia sensing using ^{15}N and ^{19}F chemical shifts.

MATERIALS AND METHODS

Synthesis of 1-(2-Fluoroethyl)-2-methyl-5-nitro-^{1}H-imidazole-$^{15}N_3$ (fluoro-[$^{15}N_3$]metronidazole). AlkylFluor was purchased from Sigma-Aldrich (P/N 900456, lot MKCJ8801). Potassium fluoride (99%), extra pure, anhydrous, was purchased from Acros Organics (P/N 201350250, lot A0415827). 1,4-Dioxane (99.5%) extra dry over a molecular sieve, AcroSeal, was purchased from Acros Organics (P/N 364341000, lot 2170684). Hexane (98.5%, P/N H292-4, lot 222209), ethyl acetate (99.5%, P/N E195-4, lot-210176), methylene chloride (99.9%, P/N D37-4, lot-221259), and methanol (99.8%, P/N A412-4, lot-223204) were purchased from Fisher chemical. Chloroform (99.8%, P/N CX1055-9, lot 59023) was purchased from EMD Millipore Corporation and used without further purification. Potassium permanganate was purchased from Alfa Aesar (98%, P/N A12170, lot M15G037).

All reactions were performed in oven-dried glassware under a positive pressure of argon or nitrogen with magnetic stirring unless otherwise mentioned. Air-sensitive reagents and solutions were transferred via syringe or cannula. Reactions were monitored by thin-layer chromatography (TLC) with 0.25 mm precoated silica gel plates (60 F254). Visualization was accomplished with either ultraviolet (UV) light or iodine staining adsorbed on silica gel. The ^{1}H and ^{13}C NMR spectra were recorded using $CDCl_3$ as solvent and TMS as internal reference. ^{1}H NMR: $CDCl_3$ (7.27); ^{13}C NMR: $CDCl_3$ (77.00). The ^{1}H and ^{13}C NMR spectra were recorded on 400 NMR (^{13}C at 100 MHz; ^{15}N at 41 MHz) spectrometers. ^{19}F NMR spectra were recorded on a 1.4 Tesla NMR spectrometer. A 400 MHz NMR spectrometer was employed for the structural characterization of the synthesized compound. The peak assignment of the product was performed using ChemDraw Professional V.16 software package. Data are reported as follows: chemical shift, multiplicity (s = singlet, d = doublet, t = triplet, m = multiplet, and br = broad), integration, and coupling constants (Hz). Column chromatographic separations were performed on silica gel (60−120 mesh and 230−400 mesh).

Compound **1** ([$^{15}N_3$]metronidazole) was synthesized by a previously reported three-step synthetic procedure.[35,36] Compound **2** (1-(2-fluoroethyl)-2-methyl-5-nitro-^{1}H-imidazole-$^{15}N_3$ or fluoro-[$^{15}N_3$]metronidazole) was synthesized by minor modifications of the reported synthesis.[37]

[$^{15}N_3$]metronidazole (261 mg, 1.5 mmol, 1.00 equiv), potassium fluoride (435.0 mg, 7.5 mmol, 5.00 equiv), and AlkylFluor (889.9 mg, 1.8 mmol, 1.20 equiv) were purged

https://doi.org/10.1021/acs.jpca.3c02317
J. Phys. Chem. A XXXX, XXX, XXX−XXX

under argon gas for 15 min in a sealed tube at room temperature, and dry 1,4-dioxane (25.0 mL) was added to the above reaction mixture under inert atmosphere. Next, the reaction mixture was purged under an argon atmosphere for 20−30 min at room temperature. Finally, the reaction mixture was heated at 40 °C for 24 h. The reaction progress was monitored by the TLC. After consumption of the starting [$^{15}N_3$]metronidazole, the reaction mixture was cooled to room temperature and concentrated in vacuo. The residue was purified by flash column chromatography on silica gel using 50% EtOAc/hexane, to afford compound **2** as a white solid (250 mg, 95%). R_f = 0.34 (ethyl acetate, $KMnO_4$ stain). The corresponding product 2 was characterized using ^{1}H, ^{13}C, and ^{19}F NMR spectroscopy. Characterization data of compound **2** were compared to literature values (see the Supporting Information for details) to confirm the identity of the product (Scheme 1).[37]

Scheme 1. Synthetic Scheme of 1-(2-Fluoroethyl)-2-methyl-5-nitro-^{1}H-imidazole-$^{15}N_3$ (Fluoro-[$^{15}N_3$]metronidazole), 2

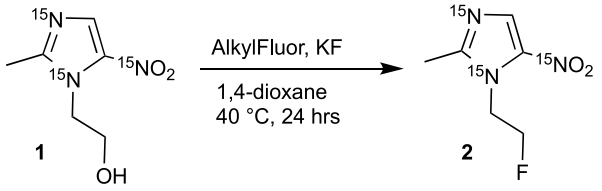

SABRE Hyperpolarization Studies. ^{15}N SABRE-SHEATH hyperpolarization was performed via a previously established procedure.[36,38] Briefly, each fluoro-[$^{15}N_3$]-metronidazole sample for SABRE hyperpolarization was prepared with a ratio 1:20 of [catalyst]/[substrate] in CD_3OD. We employed [IrCl(COD)(IMes)] (COD = *cis,cis*-1,5-cyclooctadiene, IMes = 1,3-bis(2,4,6-trimethyl-phenyl) imidazole-2-ylidene) SABRE precatalyst[39,40] for all hyperpolarization studies. The SABRE precatalyst synthesis followed the previously described procedure.[41] All described studies employed 1 mM SABRE precatalyst and 20 mM substrate (fluoro-[$^{15}N_3$]metronidazole or reference [$^{15}N_3$]-metronidazole): A measured mass of to-be-hyperpolarized substrate (fluoro-[$^{15}N_3$]metronidazole or reference [$^{15}N_3$]-metronidazole) was transferred to a plastic Eppendorf tube and mixed with CD_3OD to yield an initial concentration of 40 mM. Separately, a measured mass of SABRE precatalyst was transferred to another plastic Eppendorf tube and mixed with CD_3OD to yield an initial concentration of 2 mM. Then, 0.30 mL aliquots of each solution were mixed together to yield 1.0 and 20 mM concentrations of the precatalyst and the substrate, with the desired 1:20 [IrIMes catalyst]/[substrate] ratio. Then, the freshly prepared sample solution was transferred to a medium-wall 5 mm NMR tube (Wilmad-LabGlass, P/N 504-PP-9−5). The sample solution was then bubbled with ultrapure argon gas (>99.999%) for 1 min to remove any residual dissolved air in the solution. After the completion of the argon flush, the 5 mm NMR tube containing the prepared sample was connected to the SABRE-SHEATH hyperpolarization apparatus via 1/4" Teflon tubing as described previously.[42] A full description of the hyperpolarization apparatus was provided elsewhere.[42] Briefly, a 1/16" outer-diameter (1/32" inner-diameter) Teflon catheter was placed inside the NMR tube to deliver p-H_2 bubbles metered by the mass-flow controller (MFC) (Figure 1). The

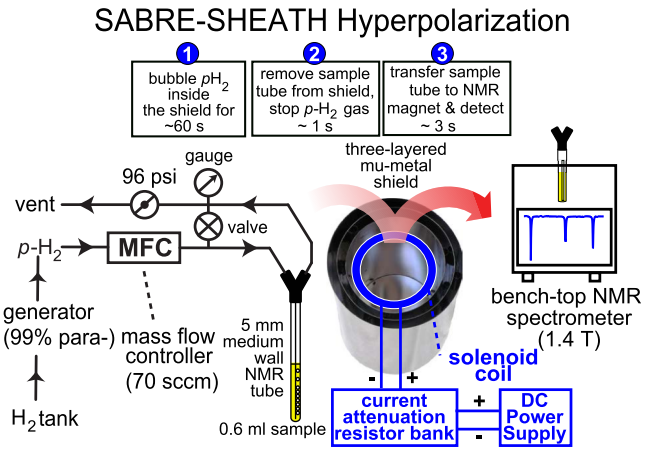

Figure 1. Experimental setup of SABRE-SHEATH hyperpolarization of fluoro-[$^{15}N_3$]metronidazole.

bubbling apparatus employs a nonmagnetic Wye 1/4"−1/8" reducing adapter (McMaster-Carr, P/N 5779K262), the second port of which is used for the exhaust of the spent hydrogen gas. Finally, the spent hydrogen gas exits the polarizer via a safety valve set to ca. 95−100 psi overpressure. All NMR data from SABRE-SHEATH hyperpolarization experiments were collected within 7 h from the beginning of the sample preparation.

Guided by the previous studies with long (tens of minutes) activation time for structurally similar [$^{15}N_3$]nimorazole,[27] the prepared precatalyst/substrate-containing solutions were bubbled with p-H_2 at a flow rate of 40 standard cubic centimeters per minute (sccm) for 2 h at 96 psi p-H_2 overpressure, corresponding to ∼8 bar total p-H_2 pressure.

SABRE[43] is a hyperpolarization technique relying on parahydrogen (p-H_2) as the source of hyperpolarization (Figure 2a). Polarization is transferred from p-H_2-derived hydrides to-be-hyperpolarized substrate ligated on a metal complex (Figure 2a). The simultaneous chemical exchange of p-H_2 and the substrate leads to a buildup of HP substrate over time. SABRE-SHEATH is performed in the microtesla magnetic fields, where the Zeeman levels of the interacting spins are matched to the spin−spin coupling between parahydrogen p-H_2-derived hydrides and the target nucleus of the substrate molecule.[34,44,45]

Following the completion of sample activation, the NMR tube containing 0.6 mL of the activated sample was placed in the center of the mu-metal shield for all SABRE-SHEATH experiments.[42,46] The temperature of the sample was maintained using a water bath placed inside the mu-metal shield. The microtesla field inside the shield was created by a solenoid coil powered by 5 VDC power supplied in series with a current-attenuation resistor bank (Figure 1). For each SABRE-SHEATH experiment, the valve shown in Figure 1 was closed to direct the gas flow through the solution in the NMR tube. All experiments were performed using a p-H_2 flow rate of 70 sccm unless noted otherwise. Upon completion of the p-H_2 bubbling, the bypass valve is opened to stop the bubbling. Finally, the sample is quickly transferred into a 1.4 T bench-top NMR spectrometer for NMR spectrum acquisition of the HP state (Figure 2b). All ^{15}N NMR spectra were recorded using a 1.4 T NMR Pro 60 (Nanalysis, Canada), whereas all ^{19}F NMR spectra were recorded using a 1.4 T SpinsolveCarbon spectrometer (Magritek, Germany-New Zealand). All bench-

https://doi.org/10.1021/acs.jpca.3c02317
J. Phys. Chem. A XXXX, XXX, XXX−XXX

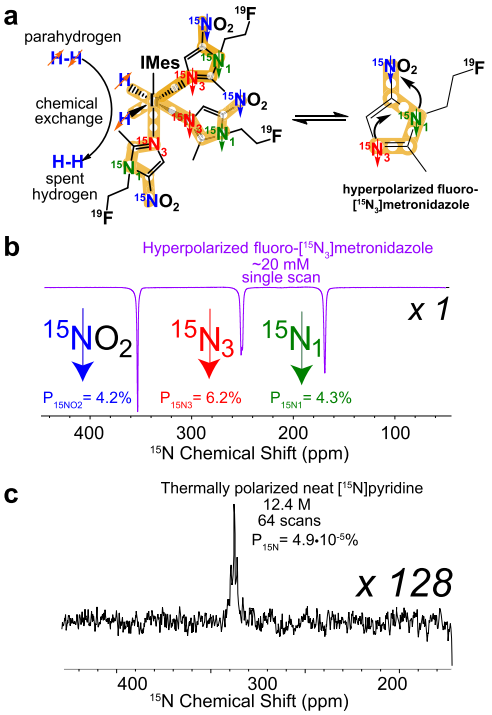

Figure 2. (a) Schematics of polarization transfer from parahydrogen-derived hydrides of the SABRE catalyst to ^{15}N nuclei of fluoro-[$^{15}N_3$]metronidazole. (b) Single-scan ^{15}N NMR spectrum of HP fluoro-[$^{15}N_3$] metronidazole. Conditions: ~20 mM substrate, ~1.0 mM catalyst, 21 °C polarization temperature, 96 psi p-H_2 overpressure, 70 sccm gas flow rate, polarization transfer magnetic field B_T of 0.73 μT. (c) ^{15}N NMR spectrum of thermally polarized neat [^{15}N]pyridine acquired with 64 signal accumulations employed as a signal reference for polarization calculation. The spectra were acquired on a 1.4 T bench-top NMR spectrometer (Nanalysis).

top NMR spectra of HP species were recorded without proton decoupling.

The signal-reference ^{15}N spectrum of thermally polarized neat [^{15}N]pyridine was recorded in the same manner (i.e., with the same parameters) as for the HP studies, except for the number of scans (64 scans vs 1) and the polarization recovery time (600 s) (Figure 2c). The signal-reference ^{19}F spectrum of thermally polarized neat ethyl trifluoroacetate (ETFA) was recorded in the same manner as the corresponding HP studies. ^{15}N and ^{19}F signal enhancement values and corresponding P_{15N} and P_{19F} polarization levels were computed as described in the Supporting Information (SI). The dynamics experiments to measure polarization buildup constant (T_b) and decay (T_1) values in microtesla fields, the Earth's field, and the field of the 1.4 T NMR spectrometer were performed as described in detail previously.[47]

DFT Calculations and ^{15}N and ^{19}F NMR Chemical Shift Computations. We have relied on the mechanism of nitroimidazole in vivo reduction in the hypoxic environment proposed by Masaki and co-workers[48] to design the structure of the corresponding metabolic intermediates for fluoro-[$^{15}N_3$]metronidazole. Specifically, stepwise enzymatic reduction of fluoro-[$^{15}N_3$]metronidazole leads to the formation of a nitroso-fluoro-[$^{15}N_3$]metronidazole intermediate, followed by the formation of a fluoro-hydroxylamino-[$^{15}N_3$]metronidazole intermediate, and finally the final product fluoro-amino-[$^{15}N_3$]metronidazole. These structures were first constructed using ChemDraw; next, each structure was loaded into GaussView software,[49] and the initial geometry optimization was performed using DFT STO-3G basis set using Gaussian'09 software.[50] Next, additional geometry optimizations were performed using the 3−21G and 6-311++g(d,p) basis sets.[51] For the DFT chemical shift tensor calculations, we employed the frequently used B3LYP functional.[52,53] The SMD solvation method (using water as the solvent) was employed for all NMR calculations. The NMR calculations of the optimized molecular geometries were calculated by a single-point GIAO method using the Pople-type basis set 6-311++g(d,p)[51] and the correction-consistent aug-cc-pVDZ Dunning basis set.[53] All ab initio calculations were performed in the ground-state geometries.[54] At the end of the calculations, the theoretically predicted isotropic chemical shielding values were converted to ^{15}N chemical shifts on an ammonia scale using the following equation:

$$\begin{aligned}\text{chemical shift} = {} & 380\ \text{ppm} - \text{Gaussian}^{15}\\ & \text{N shielding value of fluoro}\\ & -[^{15}\text{N}]\text{metronidazole} + \text{Gaussian}^{15}\\ & \text{N shielding value of}\ ^{15}\text{N} - \text{nitromethane}\end{aligned} \quad (1)$$

where 380 ppm is the experimental chemical shift of NH_4Cl on the nitromethane scale.[55] The ^{15}N shielding value of ^{15}N-nitromethane (−138.49 ppm) was computed similarly as discussed above. The theoretically calculated ^{19}F isotropic chemical shielding values were converted to ^{19}F chemical shifts on a hydrogen fluoride scale using the following equation:[56]

$$\begin{aligned}\text{chemical shift} = {} & -204\ \text{ppm}\\ & - \text{Gaussian}^{19}\text{F shielding value of fluoro}\\ & -[^{15}\text{N}_3]\text{metronidazole} + \text{Gaussian}^{19}\\ & \text{F shielding value of}\ ^{19}\text{F}\\ & - \text{hydrogen fluoride}\end{aligned} \quad (2)$$

The ab initio ^{19}F shielding value of ^{19}F nuclear spin in hydrogen fluoride was calculated to be 426.77 ppm similarly as discussed above. All of the calculated chemical shifts of ^{15}N sites and the ^{19}F site are summarized in Table S2.

RESULTS AND DISCUSSION

^{15}N SABRE-SHEATH Polarization Optimization. The efficiency of SABRE-SHEATH polarization transfer is modulated strongly by the static applied magnetic field.[26,34,44] Generally, the field mismatch in SABRE leads to suboptimal polarization transfer as the nuclear spin level anti-crossings are more separated.[57] Indeed, the sweep of the magnetic transfer field (B_T) for fluoro-[$^{15}N_3$]metronidazole reveals the P_{15N} maximum at B_T of 0.73 μT (Figure 3a). This value is in overall agreement with the optimal B_T for [$^{15}N_3$]metronidazole performed under similar experimental conditions (Figure S11b). The key difference in these field sweeps of fluoro-[$^{15}N_3$]metronidazole (compared to [$^{15}N_3$]-metronidazole) is the markedly greater P_{15N} value for the $^{15}N_3$ site relative to those for $^{15}N_1$ and $^{15}NO_2$ sites (6.2 vs 4.3% and 4.2%, respectively (Figure 2b)). In contrast, all ^{15}N polarization values for all three ^{15}N sites in [$^{15}N_3$]metronidazole have nearly identical values of ~11% (Figure S11b). A temperature sweep was performed next and revealed the

https://doi.org/10.1021/acs.jpca.3c02317
J. Phys. Chem. A XXXX, XXX, XXX−XXX

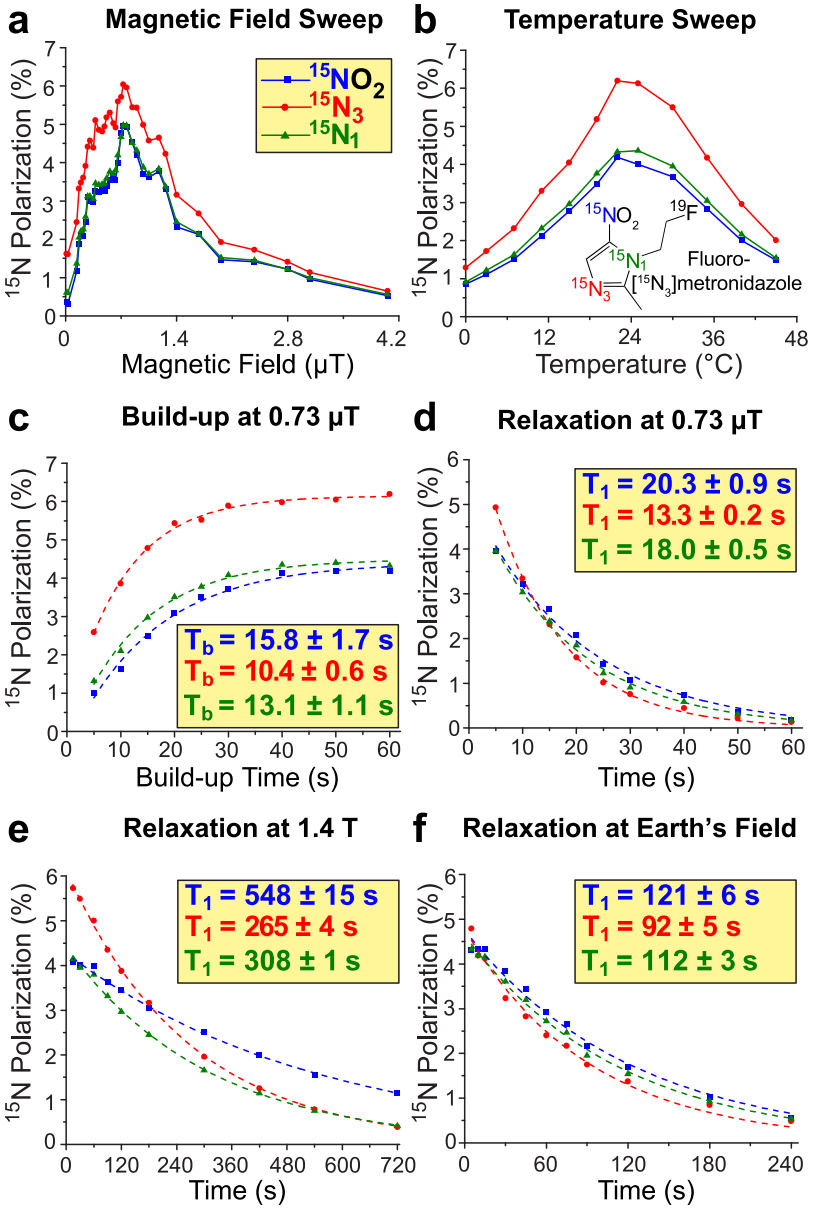

Figure 3. SABRE-SHEATH hyperpolarization of fluoro-[$^{15}N_3$] metronidazole at ~1 mM catalyst and ~20 mM substrate concentrations. (a) Magnetic field sweep of SABRE-SHEATH hyperpolarization at 22 °C. (b) Temperature sweep of SABRE-SHEATH hyperpolarization at B_T of 0.73 μT. (c) SABRE-SHEATH polarization buildup 22 °C and B_T of 0.73 μT magnetic field. (d) ^{15}N polarization decay at B_T of 0.73 μT and 22 °C. (e) ^{15}N polarization decay at 1.4 T. (f) ^{15}N polarization decay at the Earth's magnetic field. The duration of polarization buildup was 60 s unless noted otherwise.

polarization maximum for all three ^{15}N sites at 22 °C. We rationalize the observed temperature trend as follows: the most efficient polarization transfer typically occurs at the exchange rate near J, where J is the relevant spin−spin coupling between p-H_2-derived hydrides and the to-be-hyperpolarized nucleus. These observations of a clear hyperpolarization temperature maximum are in overall agreement with a wide range of other substrates studied including antifungal agents,[58] DNA bases,[59] N-heterocycles,[60] etc.[46,61] The optimized values of temperature and B_T of the SABRE-SHEATH process were employed for the relaxation dynamics studies described further below.

^{19}F SABRE-SHEATH Polarization Optimization. The overall P_{19F} value was substantially lower than those for the ^{15}N sites. Indeed, all P_{19F} values were below 0.2% (Figure 4b), i.e., approximately a factor of 20−30 lower than the P_{15N} values. This relatively low efficiency of ^{19}F SABRE-SHEATH is in good qualitative agreement with previous studies of 3-fluoro-[^{15}N]pyridine by Chukanov and co-workers.[62] The P_{19F} field sweep revealed the polarization maximum broadly centered at 1 μT (Figure 5a). The temperature sweep revealed a maximum of 28 °C, which is in overall good agreement with the optimal temperature for ^{15}N SABRE-SHEATH.

SABRE-SHEATH Relaxation Dynamics in Microtesla Magnetic Fields. We have found exponential ^{15}N polarization decay rate constants of 20.3 ± 0.9, 13.3 ± 0.2, and 18 ± 0.5 s for the $-^{15}NO_2$ group, $^{15}N_3$ and $^{15}N_1$ sites of fluoro-[$^{15}N_3$]metronidazole, respectively, at B_T of 0.73 μT (Figure 3d) (while we report these relaxation constants as "effective" T_1 values at microtesla fields, the reader is reminded that the relaxation under our experimental conditions in microtesla

https://doi.org/10.1021/acs.jpca.3c02317
J. Phys. Chem. A XXXX, XXX, XXX−XXX

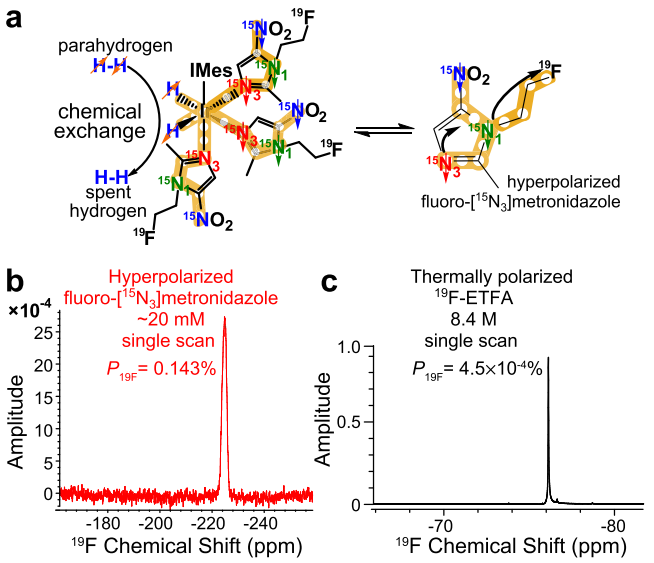

Figure 4. (a) Schematics of polarization transfer from parahydrogen-derived hydrides of the SABRE catalyst to ^{15}N nuclei of fluoro-[$^{15}N_3$]metronidazole followed by spin-relayed polarization transfer to the ^{19}F nuclear spin in microtesla magnetic fields. (b) ^{19}F NMR spectrum of HP fluoro-[$^{15}N_3$]metronidazole via SABRE-SHEATH at 21 °C, 96 psi p-H_2 overpressure, 70 sccm p-H_2 gas flow rate, and B_T of 1.4 μT. (c) ^{19}F signal-reference NMR spectrum of thermally polarized neat ethyl trifluoroacetate (ETFA). The spectra were acquired on a Spinsolve 60 NMR spectrometer.

magnetic fields is complex, and there is an interplay of near-zero-field polarization dephasing and relaxation[63]). These values are in overall qualitative agreement with the corresponding ^{15}N relaxation values for [$^{15}N_3$]metronidazole (Figure S11d and Table S1) at otherwise-identical experimental conditions. The exponential ^{15}N polarization buildup rate constants (T_b) were, respectively, found to be 15.8 ± 1.7 s for the $^{15}NO_2$ group, 10.4 ± 0.6 s for $^{15}N_3$, and 13.8 ± 1.1 s for $^{15}N_1$ in fluoro-[$^{15}N_3$]metronidazole. These values are very similar to those of [$^{15}N_3$]metronidazole (Figure S11d and Table S1) at identical experimental conditions. Moreover, in fluoro-[$^{15}N_3$]metronidazole, the ^{19}F T_1 and T_b values (16.4 ± 0.4 and 9.7 ± 1.1 s, Figure 5c,d) are comparable to those of the ^{15}N sites.

Spin-Relays in the Microtesla Magnetic Field of SABRE-SHEATH. The ^{19}F nuclear spin is seven chemical bonds away from the p-H_2-derived hydrides, and the associated seven-bond spin−spin coupling is virtually nonexistent,[64] hinting that direct polarization transfer from p-H_2-derived hydrides to the ^{19}F nucleus is likely not possible. The observations that the ^{19}F nuclear spin is hyperpolarized and that the microtesla relaxation dynamics is similar for ^{19}F and ^{15}N nuclear spins rationalized through the likely existence of a $^{15}N_3$−$^{15}N_1$(−$^{15}NO_2$)−^{19}F spin-relay, in which all ^{15}N spins are coupled via two-bond-spin−spin couplings. Moreover, the ^{19}F site is spin−spin coupled to the $^{15}N_1$ site via a three-bond spin−spin coupling of approx. 3.1 Hz.[36] Since the nuclear spin Zeeman energy levels are mixed for all nuclear spins at the near-zero magnetic field, the spin-relays effectively allow hyperpolarization to be shared between these sites for spin−spin coupled nuclear spins. The high efficiency of polarization transfer within ^{15}N−^{15}N spin-relays that has been extensively discussed elsewhere[36,65] leads to effectively the same polarization levels of all three ^{15}N sites in [$^{15}N_3$]metronidazole. The addition of spin−spin coupled ^{19}F to the spin-relays formed by ^{15}N nuclear spins in fluoro-[$^{15}N_3$]metronidazole creates another spin center that may share polarization with spin-relayed ^{15}N sites.

This notion is supported by the similar "effective" T_1 of all ^{15}N and ^{19}F sites in the microtesla fields. Of note, the "true" ^{19}F T_1 is likely substantially shorter: e.g., 5.4 ± 0.5 s at 1.4 T (Figures 5e) and 3.1 ± 0.3 s at the Earth's magnetic field (Figure 5f). The "effective" ^{19}F T_1 in microtesla fields is likely longer because polarization is constantly supplied/shared by the spin-relay from ^{15}N sites—as a result, all ^{15}N sites and the ^{19}F site relax in the decay experiment (and by extension buildup polarization in the buildup experiment) at similar rates in the microtesla field. We also speculate that the actual T_1 of ^{19}F may be substantially shorter in the microtesla fields, resulting in the overall inefficient polarization buildup of ^{19}F polarization with the bulk of the polarization "bleeding out". This model is additionally supported by three other observations: First, the overall P_{15N} values for all ^{15}N sites in fluoro-[$^{15}N_3$]metronidazole are at least a factor of 2 lower than those in [$^{15}N_3$]metronidazole as discussed above, pointing to the existence of additional mechanisms that deplete ^{15}N polarization. Second, the closest (to ^{19}F site) $^{15}N_1$ site exhibits a lower P_{15N} value (compared to that of $^{15}N_3$) because it is the nearest to the fast-relaxing ^{19}F site. As the $^{15}N_3$ site is further away and it is also the closest ^{15}N site to the hyperpolarization source (p-H_2-derived hydrides), it experiences the least of the depolarization effect of the ^{19}F in the spin-relay while also ostensibly experiencing the most efficient polarization re-supply effect from the p-H_2-derived hydrides. Third, the ^{19}F SABRE-SHEATH field sweep profile (Figure 5a) is in good overall agreement with the ^{15}N field sweep (Figure 3a), supporting the notion that the resulting ^{19}F polarization must be relayed via ^{15}N sites. We believe this model describes the presented experimental results in a good semiquantitative manner. The key limitation of the proposed four-spin-relayed model is its weakness to explain why the presence of nearby spin−spin coupled protons does not impact the spin-relay formed by $^{15}N_3$−$^{15}N_1$−$^{15}NO_2$ in [$^{15}N_3$]metronidazole, where ^{19}F nucleus is missing, but the protons are present. Future detailed mechanistic studies mapping proton microtesla relaxation are certainly warranted.

Relaxation Dynamics in the Earth's and 1.4 T Magnetic Fields. The T_1 relaxation of ^{15}N sites of fluoro-[$^{15}N_3$]metronidazole at the Earth's magnetic field was 121 ± 6, 92 ± 5, and 112 ± 3 s for the $^{15}NO_2$ group and the $^{15}N_3$ and $^{15}N_1$ sites of fluoro-[$^{15}N_3$]metronidazole, respectively (Figure 3f). These T_1 values are in good agreement with those obtained for [$^{15}N_3$]metronidazole (Figure S11f). At 1.4 T, the ^{15}N T_1 relaxation time values were remarkably long: 548 ± 15, 265 ± 4, and 308 ± 1 s for the $^{15}NO_2$, $^{15}N_3$, and $^{15}N_1$ sites of fluoro-[$^{15}N_3$]metronidazole, respectively (Figure 3e). These T_1 values are in good agreement with those obtained for [$^{15}N_3$]metronidazole (Figure S11e).[38] These long ^{15}N T_1 values could be of practical use for storing the HP state during future efforts involving contrast agent preparation, injection, and in vivo circulation.

Ab Initio Calculations of ^{15}N and ^{19}F NMR Chemical Shifts of Species in Putative In Vivo Metabolism in Anaerobic Environments. The nitroimidazole moiety, found in several prospective hypoxic metabolic probes like metronidazole,[16] undergoes a stepwise reduction in anaerobic

https://doi.org/10.1021/acs.jpca.3c02317
J. Phys. Chem. A XXXX, XXX, XXX−XXX

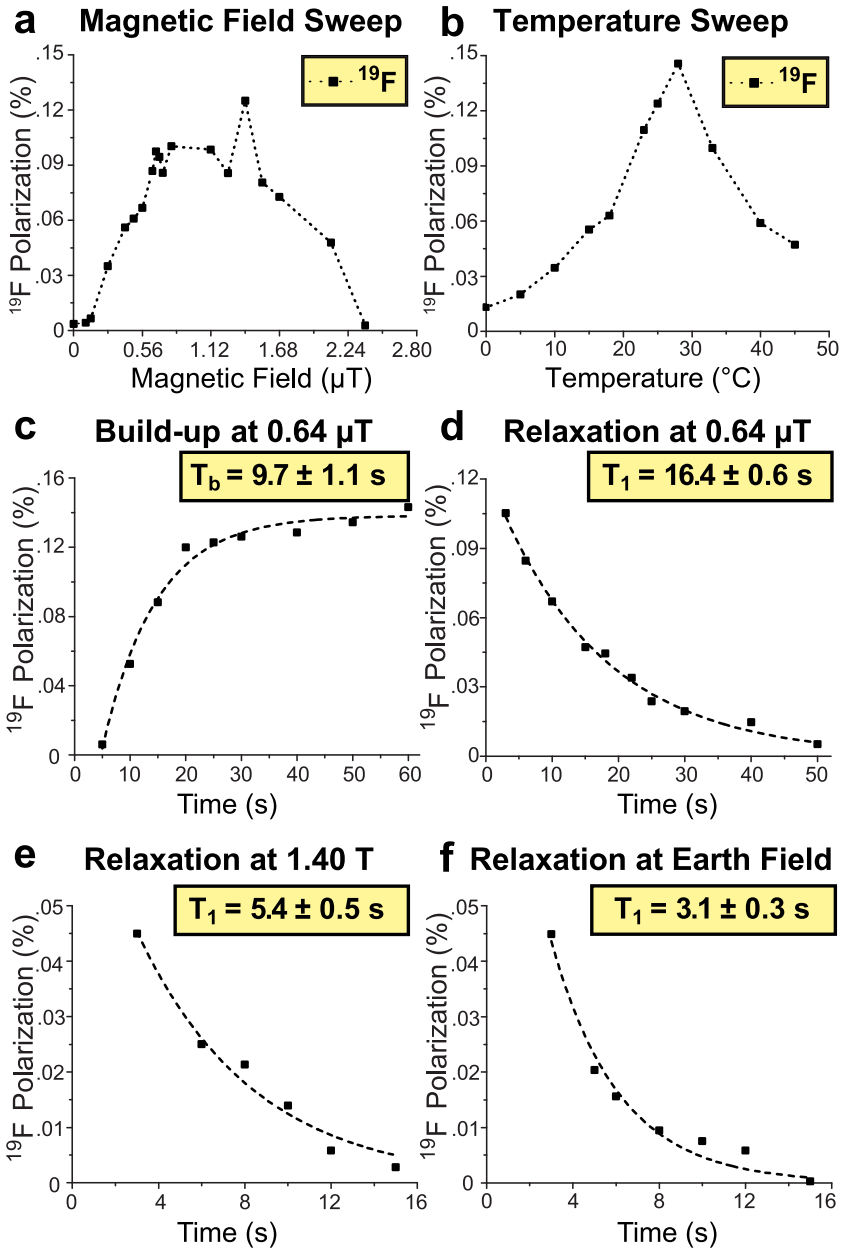

Figure 5. (a) Magnetic field dependence of the spin-relayed SABRE-SHEATH polarization transfer process for fluoro-[$^{15}N_3$]metronidazole at room temperature of ∼22 °C; (b) polarization dependence of HP fluoro-[$^{15}N_3$]metronidazole SABRE-SHEATH on the temperature at B_T of 0.64 μT; (c) ^{19}F polarization buildup curve at 0.64 μT; (d) ^{19}F polarization decay curve at 0.64 μT; (e) corresponding ^{19}F T_1 relaxation curve at 1.4 T; (f) corresponding ^{19}F T_1 relaxation curve at the Earth's magnetic field. The duration of polarization buildup was 60 s unless noted otherwise.

environments.[48,66] Because of the structural similarity, fluoro-[$^{15}N_3$]metronidazole is expected to follow the same reduction pathway under hypoxic condition (Figure 6). In this reduction process, the nitroso-derivative is formed reversibly in the first step.[48,66] This initial step is followed by the irreversible formation of the hydroxylamino and amino derivatives, as described in Figure 6. Since our long-term goal is to employ this class of compounds as novel imaging probes of hypoxia, here, we performed ab initio calculations of ^{15}N and ^{19}F isotropic chemical shifts in water. The results are summarized in Figure 6 and Table S2.

The agreement between theoretically computed chemical shift values for fluoro-[$^{15}N_3$]metronidazole in aqueous media and experimental results obtained in CD_3OD was generally good: $^{15}N_1$ (154 vs 168 ppm), $^{15}N_3$ (249 vs 253 ppm), $^{15}NO_2$ (343 vs 354 ppm), and ^{19}F (−201 vs −225 ppm). Since for chemical shift imaging applications, it is critical to spectrally resolve the metabolites, our primary interest in these calculations was to investigate the changes in the chemical shifts between the parent molecule and downstream the metabolites.

Our computational studies show that ^{15}N chemical shifts of all of the ^{15}N sites and the ^{19}F site of fluoro-[$^{15}N_3$]-metronidazole are sensitive to the reduction process. Not surprisingly, the most sensitive site was $^{15}NO_2$: $\Delta\delta$ of 393 ppm with the nitroso form, $\Delta\delta$ of −233 ppm with the hydroxylamine form, and $\Delta\delta$ of −326 ppm with the amine form. Moreover, the chemical shifts of each ^{15}N species are separated by at least 93 ppm for this site, indicating that spectroscopic differentiation of all four metabolites can be readily performed

https://doi.org/10.1021/acs.jpca.3c02317
J. Phys. Chem. A XXXX, XXX, XXX−XXX

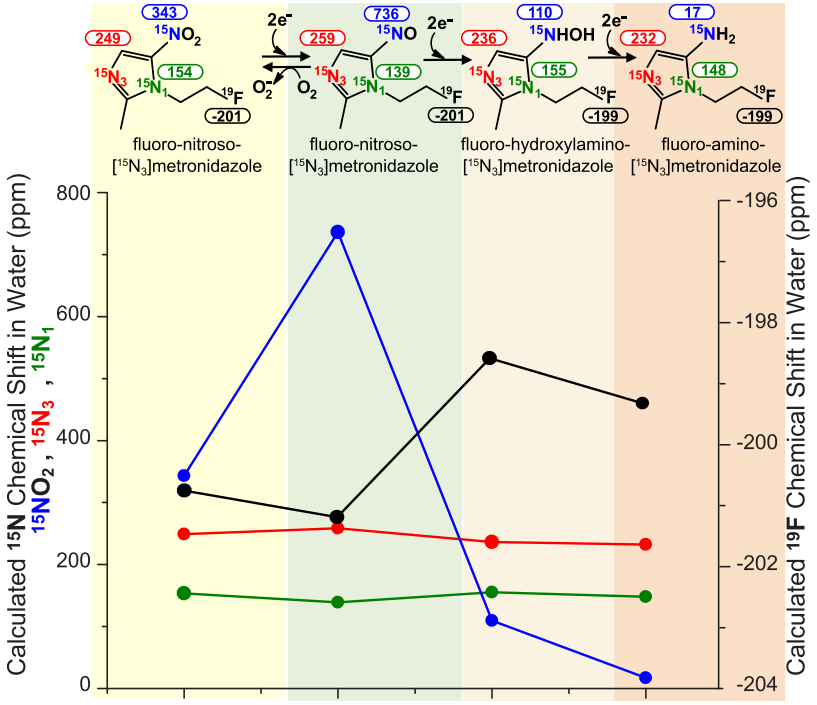

Figure 6. (Top) Schematic of putative metabolic transformations of fluoro-[$^{15}N_3$]metronidazole based on the in vivo degradation mechanism in hypoxic environments by Masaki and co-authors.[48] (Bottom) Ab initio computed ^{15}N and ^{19}F isotopic chemical shifts of putative metabolites of fluoro-[$^{15}N_3$]metronidazole based on the above mechanism. Color-coded (red, blue, and green) values of ^{15}N chemical shifts (in ppm) and black-color-coded values of ^{18}F chemical shifts (in ppm) were computed in aqueous media using Gaussian'09.

in vivo. However, the presence of directly attached protons in this site within the hydroxylamine and amine forms would likely result in a substantial decrease of their ^{15}N T_1, which may lead to rapid depolarization of this HP site in vivo—and in turn may limit its utility for metabolic sensing of the HP $^{15}NO_2$ site beyond HP ^{15}NO formation.

The second-most-sensitive site to the process of stepwise reduction is the $^{15}N_3$ site. The corresponding computed ^{15}N chemical shift changes are $\Delta\delta$ of 10 ppm with the nitroso form, $\Delta\delta$ of −13 ppm with the hydroxylamine form, and $\Delta\delta$ of −17 ppm with the amine form. Moreover, the chemical shifts of each ^{15}N species are separated by 4−13 ppm for this site, indicating that spectroscopic differentiation of all metabolites is certainly feasible in vivo. Of note, a typical in vivo spectral resolution is on the order of 1 ppm for ^{15}N magnetic resonance spectroscopy (MRS) at clinically relevant magnetic fields.[29]

The ^{15}N site that is least sensitive to the process of stepwise reduction is the $^{15}N_1$ site. The corresponding computed ^{15}N chemical shift changes are $\Delta\delta$ of −15 ppm with the nitroso form, $\Delta\delta$ of 1 ppm with the hydroxylamine form, and $\Delta\delta$ of −6 ppm with the amine form. The chemical shifts of each ^{15}N species are separated by 1−15 ppm for this site, indicating that spectroscopic detection of these metabolites is still feasible in vivo, with the exception of differentiating the injected nitro and the metabolized hydroxylamino forms—as the corresponding ^{15}N chemical shifts are nearly identical. It should be also emphasized that the chemical shifts of all three ^{15}N sites within a given structure are greatly separated from each other: for example, the $^{15}N_1$ band (139−154 ppm range) of metabolic chemical shifts is over 60 ppm away from the $^{15}N_3$ band (232−259 ppm range). This feature is important because the chemical shift dispersion of all three sites—provided these predictions are borne out—may be potentially employed for in vivo sensing of hypoxia without any concerns of signal overlap.

With respect to the ^{19}F site, there was virtually no change in chemical shift between the nitroso and nitro forms. However, there was a −2 ppm change between nitro and hydroxylamino/amino forms (Figure 6). This finding is important because it implies that the ^{19}F chemical shift may be potentially employed to sense the metabolic conversion of injected fluoro-[$^{15}N_3$]-metronidazole. Although the lifetime of the HP state of ^{19}F is too short to employ it for hyperpolarization storage (in vitro and in vivo, with T_1 = 5.4 ± 0.5 s, Figure 5e), one potential approach is to employ polarization transfer from the HP $^{15}N_1$ site to ^{19}F immediately before the ^{19}F readout. Indeed, the ∼3.1 Hz spin−spin coupling between these two sites should be sufficient for polarization transfer using INEPT or other established approaches. The feasibility of such an approach has been demonstrated for ^{13}C to ^{1}H transfer for HP [1-^{13}]-pyruvate and HP [1-^{13}C]lactate,[32] which have similar values of relevant spin−spin couplings, indicating the merit of such an approach. Given that the typical in vivo spectral resolution is ∼1 ppm or less, it may not be possible to directly spectrally resolve all putative metabolites using their ^{19}F chemical shift, since the ^{19}F chemical shift dispersion for all four species is on the order of 2 ppm. However, this narrow range does not necessarily embody a limitation for an indirect-sensing approach, as spectrally selective ^{15}N pulses may be employed to selectively excite one HP ^{15}N species at a time before performing an indirect ^{19}F readout; indeed, the predicted ^{15}N chemical shift dispersion of all four species for all ^{15}N sites is rather remarkable. This concept has been previously employed for indirect quantitative proton signal readout of ^{15}N choline metabolism.[67] Future studies are certainly warranted to evaluate the feasibility of this approach both in vitro and in

https://doi.org/10.1021/acs.jpca.3c02317
J. Phys. Chem. A XXXX, XXX, XXX−XXX

vivo—the subject of ongoing work in our collaborating laboratories. We note that performing such experiments without hyperpolarization (e.g., perfusion studies in cellular models of hypoxia) is likely extremely challenging due to the low detection sensitivity of the ^{15}N nucleus. For example, ^{15}N is ∼15 times less sensitive than ^{13}C and $\sim 10^3$ times less sensitive than protons (assuming a non-hyperpolarized state). The sensitivity issue of cellular NMR studies is often additionally exacerbated by the line-broadening suffered because of susceptibility-induced B_0 field gradients, as well as the anticipated low concentration of metabolic pathway intermediates. Nevertheless, we remain optimistic that the preparation of bio-compatible formations of HP fluoro-[$^{15}N_3$]metronidazole will enable such studies in the near future—indeed, substantial efforts are being made by the SABRE hyperpolarization community to develop such formulations.[68−70] Moreover, we anticipate that this compound can also be potentially hyperpolarized by dissolution dynamic nuclear polarization (d-DNP), thus expanding the utility of this compound to groups that practice other hyperpolarization techniques.[29]

CONCLUSIONS

We have reported on the synthesis of a potential molecular imaging probe fluoro-[$^{15}N_3$]metronidazole for hypoxia. We have employed the SABRE-SHEATH method to demonstrate hyperpolarization of ^{15}N sites with P_{15N} of 4−6%. The spin-relayed ^{19}F SABRE-SHEATH was inefficient, with $P_{19F} < 0.2\%$. As a result, the direct use of the ^{19}F hyperpolarized state (i.e., produced directly at the onset of the SABRE process) is likely not going to be useful for future in vivo studies; this notion is additionally supported by the very short ^{19}F T_1 values at the Earth's and 1.4 T fields. Therefore, the only viable strategy for potential in vivo applications is to store the HP state on the longer-lived ^{15}N sites, followed by polarization readout using ^{19}F—as discussed in greater detail above. The presence of spin-relay between ^{19}F and ^{15}N HP sites was supported by the experimental relaxation dynamics and B_T profiles. This spin-relay mechanism may lead to the reduction of ^{15}N polarization for fluoro-[$^{15}N_3$]metronidazole compared to [$^{15}N_3$]-metronidazole because the ^{19}F nucleus likely acts as a polarization sink due to short T_1 in the shield (which could not be measured in our experiment—instead, an apparent T_1 was measured as discussed above—all spin−spin-coupled nuclei share effectively the same "apparent" T_1). ^{19}F polarization is likely depressed due to efficient relaxation in microtesla magnetic fields. Long ^{15}N T_1 values of up to 9 min are reported for ^{15}N sites at a clinically relevant 1.4 T field, indicating that HP ^{15}N sites of fluoro-[$^{15}N_3$]metronidazole could be potentially employed as long-lived carriers of hyperpolarization for future in vivo studies. Although metronidazole is FDA-approved for the treatment of anaerobic bacterial infections,[71] the fluoro-[$^{15}N_3$]metronidazole variant is not FDA-approved. It should be pointed out that fluorination is now routinely used in the pharmaceutical industry to improve cancer drugs' pharmacokinetics and physiochemical properties.[72] Moreover, previous biodistribution studies with fluorinated nitroimidazoles showed no substantial difference with nonfluorinated variants.[73] Therefore, we do not envision fluorination of metronidazole to be a barrier for future translational use. To investigate the future utility of fluoro-[$^{15}N_3$]metronidazole for potential applications of hypoxia sensing, we have employed ab initio calculations to compute ^{15}N and ^{19}F chemical shifts of this potent metabolic probe and its putative metabolites resulting from the stepwise reduction process of this molecular probe in anaerobic environments. The computational studies reveal excellent ^{15}N chemical shift dispersion of all three HP ^{15}N sites of fluoro-[$^{15}N_3$]-metronidazole for delineating the metabolites. Moreover, the ^{19}F chemical shift changes induced at the ^{19}F site due to hypoxia-induced reduction processes could also be potentially useful for hypoxia sensing and detection of its metabolites. However, we note that the ab initio computational approach employed here is only a first step before future validation studies in cellular and animal models of hypoxia. The reported results reported here bode well for future studies employing this molecular probe for hypoxia sensing using ^{15}N direct MRS detection or indirect detection using ^{19}F readout.

ASSOCIATED CONTENT

Supporting Information

The Supporting Information is available free of charge at https://pubs.acs.org/doi/10.1021/acs.jpca.3c02317.

Additional experimental details of SABRE hyperpolarization studies; additional details of synthesis and spectral characterization; additional figures; description of computation studies; and log data files for ab initio calculations (PDF)

AUTHOR INFORMATION

Corresponding Authors

Mohammad S. H. Kabir − *Department of Chemistry, Wayne State University, Karmanos Cancer Institute (KCI), Detroit, Michigan 48202, United States*; Email: mshkabir@wayne.edu

Eduard Y. Chekmenev − *Department of Chemistry, Karmanos Cancer Institute (KCI), and Integrative Biosciences (Ibio), Wayne State University, Karmanos Cancer Institute (KCI), Detroit, Michigan 48202, United States; Russian Academy of Sciences, Moscow 119991, Russia;* orcid.org/0000-0002-8745-8801; Email: chekmenevlab@gmail.com

Authors

Sameer M. Joshi − *Department of Chemistry, Karmanos Cancer Institute (KCI), and Integrative Biosciences (Ibio), Wayne State University, Karmanos Cancer Institute (KCI), Detroit, Michigan 48202, United States*

Anna Samoilenko − *Department of Chemistry and Integrative Biosciences (Ibio), Wayne State University, Karmanos Cancer Institute (KCI), Detroit, Michigan 48202, United States*

Isaiah Adelabu − *Department of Chemistry and Integrative Biosciences (Ibio), Wayne State University, Karmanos Cancer Institute (KCI), Detroit, Michigan 48202, United States;* orcid.org/0000-0002-9475-0851

Shiraz Nantogma − *Department of Chemistry and Integrative Biosciences (Ibio), Wayne State University, Karmanos Cancer Institute (KCI), Detroit, Michigan 48202, United States*

Juri G. Gelovani − *Integrative Biosciences (Ibio) and Department of Biomedical Engineering, Wayne State University, Karmanos Cancer Institute (KCI), Detroit, Michigan 48202, United States; United Arab Emirates University, Al Ain, United Arab Emirates*

https://doi.org/10.1021/acs.jpca.3c02317
J. Phys. Chem. A XXXX, XXX, XXX−XXX

Boyd M. Goodson − *School of Chemical & Biomolecular Sciences, Southern Illinois University, Carbondale, Illinois 62901, United States;* orcid.org/0000-0001-6079-5077

Complete contact information is available at: https://pubs.acs.org/10.1021/acs.jpca.3c02317

Notes

The authors declare the following competing financial interest(s): EYC and BMG declare stake ownership in XeUS Technolo-gies, LTD. EYC is an equity holder of Vizma Life Sciences.

■ ACKNOWLEDGMENTS

This work was supported by the NSF under grants CHE-1904780 and CHE-1905341.

■ REFERENCES

(1) Eills, J.; Budker, D.; Cavagnero, S.; Chekmenev, E. Y.; Elliott, S. J.; Jannin, S.; Lesage, A.; Matysik, J.; Meersmann, T.; Prisner, T.; et al. Spin Hyperpolarization In Modern Magnetic Resonance. *Chem. Rev.* **2023**, *123*, 1417−1551.

(2) Nikolaou, P.; Goodson, B. M.; Chekmenev, E. Y. NMR Hyperpolarization Techniques For Biomedicine. *Chem. − Eur. J.* **2015**, *21*, 3156−3166.

(3) Mugler, J. P.; Altes, T. A. Hyperpolarized ^{129}Xe MRI Of The Human Lung. *J. Magn. Reson. Imaging* **2013**, *37*, 313−331.

(4) Brindle, K. M. Imaging Metabolism With Hyperpolarized ^{13}C-Labeled Cell Substrates. *J. Am. Chem. Soc.* **2015**, *137*, 6418−6427.

(5) Goodson, B. M. Nuclear Magnetic Resonance Of Laser-Polarized Noble Gases In Molecules, Materials, And Organisms. *J. Magn. Reson.* **2002**, *155*, 157−216.

(6) Khan, A. S.; Harvey, R. L.; Birchall, J. R.; Irwin, R. K.; Nikolaou, P.; Schrank, G.; Emami, K.; Dummer, A.; Barlow, M. J.; Goodson, B. M.; et al. Enabling Clinical Technologies For Hyperpolarized Xenon-129 MRI And Spectroscopy. *Angew. Chem., Int. Ed.* **2021**, *60*, 22126−22147.

(7) Barskiy, D. A.; Coffey, A. M.; Nikolaou, P.; Mikhaylov, D. M.; Goodson, B. M.; Branca, R. T.; Lu, G. J.; Shapiro, M. G.; Telkki, V.-V.; Zhivonitko, V. V.; et al. NMR Hyperpolarization Techniques Of Gases. *Chem. − Eur. J.* **2017**, *23*, 725−751.

(8) Grist, J. T.; Chen, M.; Collier, G. J.; Raman, B.; Abueid, G.; Mcintyre, A.; Matthews, V.; Fraser, E.; Ho, L.-P.; Wild, J. M.; et al. Hyperpolarized ^{129}Xe MRI Abnormalities In Dyspneic Participants 3 Months After COVID-19 Pneumonia: Preliminary Results. *Radiology* **2021**, *301*, E353−E360.

(9) Golman, K.; Olsson, L. E.; Axelsson, O.; Mansson, S.; Karlsson, M.; Petersson, J. S. Molecular Imaging Using Hyperpolarized C-13. *Br. J. Radiol.* **2003**, *76*, S118−S127.

(10) Kurhanewicz, J.; Vigneron, D. B.; Brindle, K.; Chekmenev, E. Y.; Comment, A.; Cunningham, C. H.; Deberardinis, R. J.; Green, G. G.; Leach, M. O.; Rajan, S. S.; et al. Analysis Of Cancer Metabolism By Imaging Hyperpolarized Nuclei: Prospects For Translation To Clinical Research. *Neoplasia* **2011**, *13*, 81−97.

(11) Merritt, M.; Harrison, C.; Storey, C.; Jeffrey, F.; Sherry, A.; Malloy, C. Hyperpolarized C-13 Allows A Direct Measure Of Flux Through A Single Enzyme-Catalyzed Step By NMR. *Proc. Natl. Acad. Sci. U.S.A.* **2007**, *104*, 19773−19777.

(12) Day, S. E.; Kettunen, M. I.; Gallagher, F. A.; Hu, D. E.; Lerche, M.; Wolber, J.; Golman, K.; Ardenkjaer-Larsen, J. H.; Brindle, K. M. Detecting Tumor Response To Treatment Using Hyperpolarized C-13 Magnetic Resonance Imaging And Spectroscopy. *Nat. Med.* **2007**, *13*, 1382−1387.

(13) Golman, K.; In't Zandt, R.; Thaning, M. Real-Time Metabolic Imaging. *Proc. Natl. Acad. Sci. U.S.A.* **2006**, *103*, 11270−11275.

(14) Kurhanewicz, J.; Vigneron, D. B.; Ardenkjaer-Larsen, J. H.; Bankson, J. A.; Brindle, K.; Cunningham, C. H.; Gallagher, F. A.; Keshari, K. R.; Kjaer, A.; Laustsen, C.; et al. Hyperpolarized ^{13}C MRI: Path To Clinical Translation In Oncology. *Neoplasia* **2019**, *21*, 1−16.

(15) Nelson, S. J.; Kurhanewicz, J.; Vigneron, D. B.; Larson, P. E. Z.; Harzstark, A. L.; Ferrone, M.; Van Criekinge, M.; Chang, J. W.; Bok, R.; Park, I.; et al. Metabolic Imaging Of Patients With Prostate Cancer Using Hyperpolarized 1-C-13 Pyruvate. *Sci. Transl. Med.* **2013**, *5*, No. 198ra108.

(16) Kizaka-Kondoh, S.; Konse-Nagasawa, H. Significance Of Nitroimidazole Compounds And Hypoxia-Inducible Factor-1 For Imaging Tumor Hypoxia. *Cancer Sci.* **2009**, *100*, 1366−1373.

(17) Hendrickson, K.; Phillips, M.; Smith, W.; Peterson, L.; Krohn, K.; Rajendran, J. Hypoxia Imaging With [F-18] FMISO-PET In Head And Neck Cancer: Potential For Guiding Intensity Modulated Radiation Therapy In Overcoming Hypoxia-Induced Treatment Resistance. *Radiother. Oncol.* **2011**, *101*, 369−375.

(18) Cheng, J.; Lei, L.; Xu, J.; Sun, Y.; Zhang, Y.; Wang, X.; Pan, L.; Shao, Z.; Zhang, Y.; Liu, G. ^{18}F-Fluoromisonidazole PET/CT: A Potential Tool For Predicting Primary Endocrine Therapy Resistance In Breast Cancer. *J. Nucl. Med.* **2013**, *54*, 333−340.

(19) Fleming, I. N.; Manavaki, R.; Blower, P. J.; West, C.; Williams, K. J.; Harris, A. L.; Domarkas, J.; Lord, S.; Baldry, C.; Gilbert, F. J. Imaging Tumour Hypoxia With Positron Emission Tomography. *Br. J. Cancer* **2015**, *112*, 238−250.

(20) Gerstner, E. R.; Zhang, Z.; Fink, J. R.; Muzi, M.; Hanna, L.; Greco, E.; Prah, M.; Schmainda, K. M.; Mintz, A.; Kostakoglu, L.; et al. Acrin 6684: Assessment Of Tumor Hypoxia In Newly Diagnosed Glioblastoma Using ^{18}F-FMISO PET And MRI. *Clin. Cancer Res.* **2016**, *22*, 5079−5086.

(21) Peers, C.; Dallas, M. L.; Boycott, H. E.; Scragg, J. L.; Pearson, H. A.; Boyle, J. P. Hypoxia And Neurodegeneration. *Ann. N. Y. Acad. Sci.* **2009**, *1177*, 169−177.

(22) Jain, R. K. Normalization Of Tumor Vasculature: An Emerging Concept In Antiangiogenic Therapy. *Science* **2005**, *307*, 58−62.

(23) Jain, R. K. Antiangiogenesis Strategies Revisited: From Starving Tumors To Alleviating Hypoxia. *Cancer Cell* **2014**, *26*, 605−622.

(24) Sachpekidis, C.; Thieke, C.; Askoxylakis, V.; Nicolay, N. H.; Huber, P. E.; Thomas, M.; Dimitrakopoulou, G.; Debus, J.; Haberkorn, U.; Dimitrakopoulou-Strauss, A. Combined Use Of (18)F-FDG And (18)F-FMISO In Unresectable Non-Small Cell Lung Cancer Patients Planned For Radiotherapy: A Dynamic PET/CT Study. *Am. J. Nucl. Med. Mol. Imaging* **2015**, *5*, 127−142.

(25) Schwartz, J.; Grkovski, M.; Rimner, A.; Schöder, H.; Zanzonico, P. B.; Carlin, S. D.; Staton, K. D.; Humm, J. L.; Nehmeh, S. A. Pharmacokinetic Analysis Of Dynamic ^{18}F-Fluoromisonidazole PET Data In Non−Small Cell Lung Cancer. *J. Nucl. Med.* **2017**, *58*, 911−919.

(26) Barskiy, D. A.; Shchepin, R. V.; Coffey, A. M.; Theis, T.; Warren, W. S.; Goodson, B. M.; Chekmenev, E. Y. Over 20% ^{15}N Hyperpolarization In Under One Minute For Metronidazole, An Antibiotic And Hypoxia Probe. *J. Am. Chem. Soc.* **2016**, *138*, 8080−8083.

(27) Salnikov, O. G.; Chukanov, N. V.; Svyatova, A.; Trofimov, I. A.; Kabir, M. S. H.; Gelovani, J. G.; Kovtunov, K. V.; Koptyug, I. V.; Chekmenev, E. Y. ^{15}N NMR Hyperpolarization Of Radiosensitizing Antibiotic Nimorazole Via Reversible Parahydrogen Exchange In Microtesla Magnetic Fields. *Angew. Chem., Int. Ed.* **2021**, *60*, 2406−2413.

(28) Cudalbu, C.; Comment, A.; Kurdzesau, F.; Van Heeswijk, R. B.; Uffmann, K.; Jannin, S.; Denisov, V.; Kirik, D.; Gruetter, R. Feasibility Of In Vivo N-15 MRS Detection Of Hyperpolarized N-15 Labeled Choline In Rats. *Phys. Chem. Chem. Phys.* **2010**, *12*, 5818−5823.

(29) Park, H.; Wang, Q. State-Of-The-Art Accounts Of Hyperpolarized ^{15}N-Labeled Molecular Imaging Probes For Magnetic Resonance Spectroscopy And Imaging. *Chem. Sci.* **2022**, *13*, 7378−7391.

(30) Sarkar, R.; Comment, A.; Vasos, P. R.; Jannin, S.; Gruetter, R.; Bodenhausen, G.; Hall, H.; Kirik, D.; Denisov, V. P. Proton NMR Of N-15-Choline Metabolites Enhanced By Dynamic Nuclear Polarization. *J. Am. Chem. Soc.* **2009**, *131*, 16014−16015.

(31) Chekmenev, E. Y.; Norton, V. A.; Weitekamp, D. P.; Bhattacharya, P. Hyperpolarized ^{1}H NMR Employing Low Gamma Nucleus For Spin Polarization Storage. *J. Am. Chem. Soc.* **2009**, *131*, 3164−3165.
(32) Wang, J.; Kreis, F.; Wright, A. J.; Hesketh, R. L.; Levitt, M. H.; Brindle, K. M. Dynamic ^{1}H Imaging Of Hyperpolarized [1-^{13}C]-Lactate In Vivo Using A Reverse Inept Experiment. *Magn. Reson. Med.* **2018**, *79*, 741−747.
(33) Truong, M. L.; Coffey, A. M.; Shchepin, R. V.; Waddell, K. W.; Chekmenev, E. Y. Sub-Second Proton Imaging Of ^{13}C Hyperpolarized Contrast Agents In Water. *Contrast Media Mol. Imaging* **2014**, *9*, 333−341.
(34) Theis, T.; Truong, M. L.; Coffey, A. M.; Shchepin, R. V.; Waddell, K. W.; Shi, F.; Goodson, B. M.; Warren, W. S.; Chekmenev, E. Y. Microtesla SABRE Enables 10% Nitrogen-15 Nuclear Spin Polarization. *J. Am. Chem. Soc.* **2015**, *137*, 1404−1407.
(35) Chukanov, N. V.; Shchepin, R. V.; Joshi, S. M.; Kabir, M. S. H.; Salnikov, O. G.; Svyatova, A.; Koptyug, I. V.; Gelovani, J. G.; Chekmenev, E. Y. Synthetic Approaches For ^{15}N-Labeled Hyperpolarized Heterocyclic Molecular Imaging Agents For ^{15}N NMR Signal Amplification By Reversible Exchange In Microtesla Magnetic Fields. *Chem. − Eur. J.* **2021**, *27*, 9727−9736.
(36) Shchepin, R. V.; Birchall, J. R.; Chukanov, N. V.; Kovtunov, K. V.; Koptyug, I. V.; Theis, T.; Warren, W. S.; Gelovani, J. G.; Goodson, B. M.; Shokouhi, S.; et al. Hyperpolarizing Concentrated Metronidazole $^{15}NO_2$ Group Over Six Chemical Bonds With More Than 15% Polarization And 20 Minute Lifetime. *Chem. − Eur. J.* **2019**, *25*, 8829−8836.
(37) Goldberg, N. W.; Shen, X.; Li, J.; Ritter, T. Alkylfluor: Deoxyfluorination Of Alcohols. *Org. Lett.* **2016**, *18*, 6102−6104.
(38) Birchall, J. R.; Kabir, M. S. H.; Salnikov, O. G.; Chukanov, N. V.; Svyatova, A.; Kovtunov, K. V.; Koptyug, I. V.; Gelovani, J. G.; Goodson, B. M.; Pham, W.; Chekmenev, E. Y. Quantifying The Effects Of Quadrupolar Sinks Via ^{15}N Relaxation Dynamics In Metronidazoles Hyperpolarized Via SABRE-SHEATH. *Chem. Commun.* **2020**, *56*, 9098−9101.
(39) Cowley, M. J.; Adams, R. W.; Atkinson, K. D.; Cockett, M. C. R.; Duckett, S. B.; Green, G. G. R.; Lohman, J. A. B.; Kerssebaum, R.; Kilgour, D.; Mewis, R. E. Iridium N-Heterocyclic Carbene Complexes As Efficient Catalysts For Magnetization Transfer From Para-Hydrogen. *J. Am. Chem. Soc.* **2011**, *133*, 6134−6137.
(40) Vazquez-Serrano, L. D.; Owens, B. T.; Buriak, J. M. The Search For New Hydrogenation Catalyst Motifs Based On N-Heterocyclic Carbene Ligands. *Inorg. Chim. Acta* **2006**, *359*, 2786−2797.
(41) Barskiy, D. A.; Kovtunov, K. V.; Koptyug, I. V.; He, P.; Groome, K. A.; Best, Q. A.; Shi, F.; Goodson, B. M.; Shchepin, R. V.; Coffey, A. M.; et al. The Feasibility Of Formation And Kinetics Of NMR Signal Amplification By Reversible Exchange (SABRE) At High Magnetic Field (9.4 T). *J. Am. Chem. Soc.* **2014**, *136*, 3322−3325.
(42) Joalland, B.; Nantogma, S.; Chowdhury, M. R. H.; Nikolaou, P.; Chekmenev, E. Y. Magnetic Shielding Of Parahydrogen Hyperpolarization Experiments For The Masses. *Magn. Reson. Chem.* **2021**, *59*, 1180−1186.
(43) Adams, R. W.; Aguilar, J. A.; Atkinson, K. D.; Cowley, M. J.; Elliott, P. I. P.; Duckett, S. B.; Green, G. G. R.; Khazal, I. G.; Lopez-Serrano, J.; Williamson, D. C. Reversible Interactions With Para-Hydrogen Enhance NMR Sensitivity By Polarization Transfer. *Science* **2009**, *323*, 1708−1711.
(44) Shchepin, R. V.; Truong, M. L.; Theis, T.; Coffey, A. M.; Shi, F.; Waddell, K. W.; Warren, W. S.; Goodson, B. M.; Chekmenev, E. Y. Hyperpolarization Of "Neat" Liquids By NMR Signal Amplification By Reversible Exchange. *J. Phys. Chem. Lett.* **2015**, *6*, 1961−1967.
(45) Truong, M. L.; Theis, T.; Coffey, A. M.; Shchepin, R. V.; Waddell, K. W.; Shi, F.; Goodson, B. M.; Warren, W. S.; Chekmenev, E. Y. ^{15}N Hyperpolarization By Reversible Exchange Using SABRE-SHEATH. *J. Phys. Chem. C* **2015**, *119*, 8786−8797.
(46) Adelabu, I.; Tomhon, P.; Kabir, M. S. H.; Nantogma, S.; Abdulmojeed, M.; Mandzhieva, I.; Ettedgui, J.; Swenson, R. E.; Krishna, M. C.; Theis, T.; et al. Order-Unity ^{13}C Nuclear Polarization Of [1-^{13}C]Pyruvate In Seconds And The Interplay Of Water And SABRE Enhancement. *ChemPhysChem* **2022**, *23*, 131−136.
(47) Adelabu, I.; Chowdhury, M. R. H.; Nantogma, S.; Oladun, C.; Ahmed, F.; Stilgenbauer, L.; Sadagurski, M.; Theis, T.; Goodson, B. M.; Chekmenev, E. Y. Efficient SABRE-SHEATH Hyperpolarization Of Potent Branched-Chain-Amino-Acid Metabolic Probe [1-^{13}C]-Ketoisocaproate. *Metabolites* **2023**, *13*, No. 200.
(48) Masaki, Y.; Shimizu, Y.; Yoshioka, T.; Tanaka, Y.; Nishijima, K.-I.; Zhao, S.; Higashino, K.; Sakamoto, S.; Numata, Y.; Yamaguchi, Y.; et al. The Accumulation Mechanism Of The Hypoxia Imaging Probe "FMISO" By Imaging Mass Spectrometry: Possible Involvement Of Low-Molecular Metabolites. *Sci. Rep.* **2015**, *5*, No. 16802.
(49) Dennington, R.; Keith, T. A.; Millam, J. M. *Gaussview*, version 6; Semichem Inc.: Shawnee Mission, KS, 2016.
(50) Frisch, M. J.; Trucks, G. W.; Schlegel, H. B.; Scuseria, G. E.; Robb, M. A.; Cheeseman, J. R.; Scalmani, G.; Barone, V.; Petersson, G. A.; Nakatsuji, H.et al. *Gaussian'09*; Gaussian, Inc.: Wallingford, CT, 2016.
(51) Hariharan, P. C.; Pople, J. A. The Influence Of Polarization Functions On Molecular Orbital Hydrogenation Energies. *Theor. Chim. Acta* **1973**, *28*, 213−222.
(52) Becke, A. D. Density-Functional Exchange-Energy Approximation With Correct Asymptotic Behavior. *Phys. Rev. A* **1988**, *38*, 3098−3100.
(53) Dunning, T. H. Gaussian Basis Sets For Use In Correlated Molecular Calculations. I. The Atoms Boron Through Neon And Hydrogen. *J. Chem. Phys.* **1989**, *90*, 1007−1023.
(54) Benzi, C.; Crescenzi, O.; Pavone, M.; Barone, V. Reliable NMR Chemical Shifts For Molecules In Solution By Methods Rooted In Density Functional Theory. *Magn. Reson. Chem.* **2004**, *42*, S57−S67.
(55) Pace, V.; Holzer, W.; Ielo, L.; Shi, S.; Meng, G.; Hanna, M.; Szostak, R.; Szostak, M. ^{17}O NMR And ^{15}N NMR Chemical Shifts Of Sterically-Hindered Amides: Ground-State Destabilization In Amide Electrophilicity. *Chem. Commun.* **2019**, *55*, 4423−4426.
(56) Ebrahimi, H. P.; Tafazzoli, M. An Approach To Evaluation Of ^{19}F-NMR Chemical Shifts Via Basis Functions Analysis In Fluorinated Small Compounds. *Concept Magn. Reson., Part A* **2012**, *40A*, 192−204.
(57) Pravdivtsev, A. N.; Yurkovskaya, A. V.; Vieth, H.-M.; Ivanov, K. L. Spin Mixing At Level Anti-Crossings In The Rotating Frame Makes High-Field SABRE Feasible. *Phys. Chem. Chem. Phys.* **2014**, *16*, 24672−24675.
(58) Macculloch, K.; Tomhon, P.; Browning, A.; Akeroyd, E.; Lehmkuhl, S.; Chekmenev, E. Y.; Theis, T. Hyperpolarization Of Common Antifungal Agents With SABRE. *Magn. Reson. Chem.* **2021**, *59*, 1225−1235.
(59) Kidd, B. E.; Gemeinhardt, M. E.; Mashni, J. A.; Gesiorski, J. L.; Bales, L. B.; Limbach, M. N.; Shchepin, R. V.; Kovtunov, K. V.; Koptyug, I. V.; Chekmenev, E. Y.; Goodson, B. M. Hyperpolarizing DNA Nucleobases Via NMR Signal Amplification By Reversible Exchange. *Molecules* **2023**, *28*, No. 1198.
(60) Shchepin, R. V.; Barskiy, D. A.; Coffey, A. M.; Theis, T.; Shi, F.; Warren, W. S.; Goodson, B. M.; Chekmenev, E. Y. ^{15}N Hyperpolarization Of Imidazole-$^{15}N_2$ For Magnetic Resonance Ph Sensing Via SABRE-SHEATH. *ACS Sens.* **2016**, *1*, 640−644.
(61) Tomhon, P.; Abdulmojeed, M.; Adelabu, I.; Nantogma, S.; Kabir, M. S. H.; Lehmkuhl, S.; Chekmenev, E. Y.; Theis, T. Temperature Cycling Enables Efficient ^{13}C SABRE-SHEATH Hyperpolarization And Imaging Of [1-^{13}C]-Pyruvate. *J. Am. Chem. Soc.* **2022**, *144*, 282−287.
(62) Chukanov, N. V.; Salnikov, O. G.; Shchepin, R. V.; Svyatova, A.; Kovtunov, K. V.; Koptyug, I. V.; Chekmenev, E. Y. ^{19}F Hyperpolarization Of ^{15}N-3-^{19}F-Pyridine Via Signal Amplification By Reversible Exchange. *J. Phys. Chem. C* **2018**, *122*, 23002−23010.
(63) Nantogma, S.; Eriksson, S. L.; Adelabu, I.; Mandzhieva, I.; Browning, A.; Tomhon, P.; Warren, W. S.; Theis, T.; Goodson, B. M.; Chekmenev, E. Y. Interplay Of Near-Zero-Field Dephasing, Rephasing, And Relaxation Dynamics And [1-^{13}C]Pyruvate Polar-

https://doi.org/10.1021/acs.jpca.3c02317
J. Phys. Chem. A XXXX, XXX, XXX−XXX

ization Transfer Efficiency In Pulsed SABRE-SHEATH. *J. Phys. Chem. A* **2022**, *126*, 9114−9123.
(64) Eshuis, N.; Aspers, R. L. E. G.; Van Weerdenburg, B. J. A.; Feiters, M. C.; Rutjes, F. P. J. T.; Wijmenga, S. S.; Tessari, M. Determination Of Long-Range Scalar $^{1}H-^{1}H$ Coupling Constants Responsible For Polarization Transfer In SABRE. *J. Magn. Reson.* **2016**, *265*, 59−66.
(65) Shchepin, R. V.; Jaigirdar, L.; Theis, T.; Warren, W. S.; Goodson, B. M.; Chekmenev, E. Y. Spin Relays Enable Efficient Long-Range Heteronuclear Signal Amplification By Reversible Exchange. *J. Phys. Chem. C* **2017**, *121*, 28425−28434.
(66) Masaki, Y.; Shimizu, Y.; Yoshioka, T.; Feng, F.; Zhao, S.; Higashino, K.; Numata, Y.; Kuge, Y. Imaging Mass Spectrometry Revealed The Accumulation Characteristics Of The 2-Nitroimidazole-Based Agent "Pimonidazole" In Hypoxia. *PLoS One* **2016**, *11*, No. E0161639.
(67) Harris, T.; Giraudeau, P.; Frydman, L. Kinetics From Indirectly Detected Hyperpolarized NMR Spectroscopy By Using Spatially Selective Coherence Transfers. *Chem. − Eur. J.* **2011**, *17*, 697−703.
(68) Schmidt, A. B.; De Maissin, H.; Adelabu, I.; Nantogma, S.; Ettedgui, J.; Tomhon, P.; Goodson, B. M.; Theis, T.; Chekmenev, E. Y. Catalyst-Free Aqueous Hyperpolarized [1-^{13}C]Pyruvate Obtained By Re-Dissolution Signal Amplification By Reversible Exchange. *ACS Sens.* **2022**, *7*, 3430−3439.
(69) De Maissin, H.; Groß, P.; Mohiuddin, O.; Weigt, M.; Nagel, L.; Herzog, M.; Wang, Z.; Willing, R.; Reichardt, W.; Pichotka, M.et al.In Vivo Metabolic Imaging Of [1-^{13}C]Pyruvate-D3 Hyperpolarized By Reversible Exchange With Parahydrogen. *Chemrxiv* 2023 DOI: 10.26434/Chemrxiv-2023-9trxb.
(70) Browning, A.; Macculloch, K.; Guarin, B. D.; Dedesma, C.; Goodson, B. M.; Rosen, M. S.; Chekmenev, E. Y.; Yen, Y.-F.; Tomhon, P.; Theis, T.Facile Hyperpolarization Chemistry For Molecular Imaging And Metabolic Tracking Of [1-^{13}C]Pyruvate In Vivo. *Chemrxiv* 2023 DOI: 10.26434/Chemrxiv-2023-4dqkx.
(71) Roy, R. B.; Laird, S. M.; Heasman, L. Treatment Of Trichomoniasis In The Female. A Comparison Of Metronidazole And Nimorazole. *Sex. Transm. Infect.* **1975**, *51*, 281−284.
(72) Isanbor, C.; O'Hagan, D. Fluorine In Medicinal Chemistry: A Review Of Anti-Cancer Agents. *J. Fluorine Chem.* **2006**, *127*, 303−319.
(73) Jerabek, P. A.; Patrick, T. B.; Kilbourn, M. R.; Dischino, D. D.; Welch, M. J. Synthesis And Biodistribution Of ^{18}F-Labeled Fluoronitroimidazoles: Potential In Vivo Markers Of Hypoxic Tissue. *Int. J. Radiat. Appl. Instrum., Part A Appl. Radiat. Isot.* **1986**, *37*, 599−605.

https://doi.org/10.1021/acs.jpca.3c02317
J. Phys. Chem. A XXXX, XXX, XXX−XXX